Nonlinear quasilocalized excitations in glasses

True representatives of soft spots

Kapteijns, G.; Richard, D.; Lerner, E.

Link to publication

Nonlinear quasilocalized excitations in glasses: True representatives of soft spots

Geert Kapteijns,[1] David Richard,[1,2] and Edan Lerner [1]

[1]*Institute for Theoretical Physics, University of Amsterdam, Science Park 904, Amsterdam, The Netherlands*
[2]*Department of Physics, Syracuse University, Syracuse, New York 13244, USA*

Structural glasses formed by quenching a melt possess a population of soft quasilocalized excitations—often called "soft spots"—that are believed to play a key role in various thermodynamic, transport, and mechanical phenomena. Under a narrow set of circumstances, quasilocalized excitations assume the form of vibrational (normal) modes, that are readily obtained by a harmonic analysis of the multidimensional potential energy. In general, however, direct access to the population of quasilocalized modes via harmonic analysis is hindered by hybridizations with other low-energy excitations, e.g., phonons. In this series of papers we reintroduce and investigate the statistical-mechanical properties of a class of low-energy quasilocalized modes—coined here *nonlinear quasilocalized excitations* (NQEs)—that are defined via an anharmonic (nonlinear) analysis of the potential-energy landscape of a glass, and do not hybridize with other low-energy excitations. In this paper, we review the theoretical framework that embeds a micromechanical definition of NQEs. We demonstrate how harmonic quasilocalized modes hybridize with other soft excitations, whereas NQEs properly represent soft spots without hybridization. We show that NQEs' energies converge to the energies of the softest, nonhybridized harmonic quasilocalized modes, cementing their status as true representatives of soft spots in structural glasses. Finally, we perform a statistical analysis of the mechanical properties of NQEs, which results in a prediction for the distribution of potential-energy barriers that surround typical inherent states of structural glasses, as well as a prediction for the distribution of local strain thresholds to plastic instability.

I. INTRODUCTION

A major goal in the past and current investigations of structural glasses is revealing and understanding the statistical-mechanical properties of low-energy excitations [1–19], and the role these excitations play in various thermodynamic [20–22], mechanical [23,24], transport [22,25,26], and yielding phenomena [27–31], as well as their connection to dynamics in the viscous supercooled liquid state [32–34].

It is now well accepted that, at the lowest energies, glasses feature two types of excitations. First, there are elastic waves (phonons), that must emerge due to the translational invariance of the potential energy [35] and are predicted within (linear) continuum elasticity theory. While phonons in glasses are imperfect due to the structural and mechanical disorder [36], the density of phonons of frequency ω nevertheless follows the Debye prediction $D(\omega) \sim \omega^{\bar{d}-1}$ in $\bar{d}$ spatial dimensions [37].

Second, glasses feature a population of soft, nonphononic quasilocalized modes (QLMs) that arises due to glasses' microscopic disorder and mechanical frustration, as established decades ago using computer simulations [4–6], and also argued for on theoretical grounds [1–3]. In computer glasses, these excitations are cleanly revealed as harmonic vibrational (normal) modes (see definition below) either below [13] or between [14,18] phonon bands, namely, in the absence of strong hybridizations. In these circumstances, the nonphononic modes follow a universal gapless density of states $\mathcal{D}(\omega) \sim \omega^4$ in the limit $\omega \to 0$ [13,18], and are *quasilocalized*—they consist of a localized, disordered core,

dressed by an Eshelby-like algebraic decay away from the core [13]. The universal law $\mathcal{D}(\omega) \sim \omega^4$ was shown to be independent of spatial dimension [16], microscopic details [13], and glass preparation protocol (e.g., cooling rate) [15,38]. The universal distribution even persists in the most deeply supercooled computer glasses [17,19].

It is precisely this population of soft QLMs, and their interaction with phonons, that is thought to influence various unexplained universal phenomena that are specific to structural glasses [20–22,26]. Furthermore, a subset of QLMs was shown to represent the carriers of plasticity in externally loaded glasses [30,31,39], and might be key in determining relaxation patterns in supercooled liquids [32–34]. Therefore, knowledge of their full distribution is crucial for advancing our fundamental understanding of many glassy phenomena.

However, as noted above, in a normal mode analysis, localized soft spots assume the form of harmonic vibrational modes only when hybridizations with other low-frequency excitations—in particular with phonons [8]—do not occur. It has been shown in [36] that, in the thermodynamic limit, phonons dominate glasses' low-frequency spectra, and hybridization of QLMs and phonons is inevitable. This makes it impossible to cleanly observe QLMs assuming the form of harmonic modes in that limit, which is a severe limitation of the harmonic analysis as a useful investigative tool of soft QLMs. We emphasize that the existence of QLMs—as anomalously soft spots in the glass—and their effect on various physical phenomena are *not* dependent on whether they can be realized as harmonic modes or not (as shown e.g., in [39]).
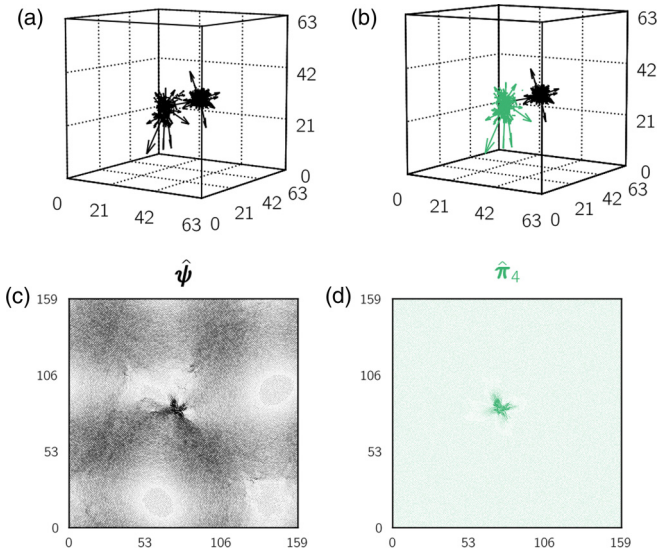
FIG. 1. NQEs are indifferent to hybridization with excitations of nearby frequencies. Panel (a) shows a normal mode that consists of two hybridized quasilocalized excitations of similar frequency. In panel (b), we show that these excitations are cleanly separated as two NQEs. Panel (c) shows a normal mode that is a mixture of a quasilocalized excitation and a nearby phononic excitation; panel (d) shows the dehybridized NQE. In panels (a) and (b), only the largest 0.1% of components of each mode is shown. For visual purposes, the modes are scaled so that the largest component of the NQE is the same size as the corresponding component of the harmonic mode.

Recently, a theoretical framework was introduced [14] (which will be summarized in Sec. III below) that formulates quasilocalized excitations in a *nonlinear* way—outside of the normal (linear) mode analysis—such that they are *indifferent* to hybridizations with phonons or with other quasilocalized excitations of nearby frequencies. The robustness of these *nonlinear quasilocalized excitations* (NQEs) against hybridizations is demonstrated in Fig. 1; in the left panels we show low-frequency *harmonic* modes measured in generic computer glasses, which consist of *two* hybridized localized soft spots [panel (a)], and a localized soft spot hybridized with a phonon [panel (c)]. In panel (b) we show that *each* of the hybridized soft spots from panel (a) is represented by a *different* NQE, while panel (d) shows that the soft spot that is hybridized with a phonon in panel (c) is represented by a single NQE, with no wavelike background (see Appendix B for details about the calculation of normal modes and NQEs).

In this series of papers we present a comprehensive study of the statistical, mechanical, and statistical-mechanical properties of NQEs, together with a methodological framework that enables the calculation of NQEs in generic computer glasses. We also extensively discuss the implications of our findings towards understanding some of the aforementioned fundamental and unresolved problems in glass physics.

In this first paper, in Sec. III we reintroduce—in simple, physically transparent terms—the theoretical framework from which a micromechanical definition of NQEs emerges. We then demonstrate in Sec. IV that NQEs are true representatives of soft spots in structural glasses: we show that NQEs

TABLE I. Ensemble size for each system size N for the 2D IPL, 3D IPL, and 4D IPL models.

	2D IPL				3D IPL			4D IPL
N	400	1600	6400	25600	2048	8192	32768	10000
Ensemble size	10 K	10 K	10 K	10 K	320 K	80 K	20 K	2 K

disentangle localized soft spots from hybridized harmonic modes, and discuss in detail the energetic properties of NQEs compared to their harmonic counterparts. In Sec. V, we put forward several key observations regarding the mechanical properties of NQEs, which enable important predictions about two fundamental properties of structural glasses: (i) glasses' destabilization under externally imposed deformations and (ii) the form of the distribution of potential-energy barriers that surround typical inherent states (local minima of the potential U) of a generic glass. Finally, in Sec. VI we discuss several avenues for future investigations, and look ahead to the other papers in this series. Our notation conventions are explained in Appendix A, and we describe in detail how NQEs are calculated in Appendix B.

II. COMPUTER GLASS MODELS

In this paper, we employ two different glass-forming models. For most of the results reported below (and when not reported otherwise), data are shown for the inverse-power-law model, which we refer to as the IPL model from now on. It is a 50:50 binary mixture of "large" and "small" particles interacting with a pairwise potential $U(r) \sim r^{-10}$. The full details of this model, including microscopic units, elastic properties, cutoff radius, and additional smoothing terms, are provided in [40]. In three dimensions (3D), we create glassy samples by performing an instantaneous quench from equilibrium liquid configurations at $T = 2.0$, which is 2.5 times larger than the temperature at which the athermal shear modulus of the underlying inherent states starts to saturate. We also study two-dimensional (2D) and four-dimensional (4D) glasses, prepared with the protocol described in [16]. We report the number of generated samples for each system size and spatial dimension in Table I.

To study the effect of preparation protocol, we additionally employ a highly polydisperse inverse-power-law model [41], that is optimized so that it can be extremely efficiently equilibrated with the Swap Monte Carlo algorithm [42–44], while remaining robust against crystallization. We use a slightly modified version of the model presented in [41], the details of which are given in [40], which we refer to as the POLY model. We prepare glassy samples by performing an instantaneous quench from equilibrium liquid configurations at three different temperatures: $T = 0.35$ (deeply supercooled), $T = 0.5$ (moderately supercooled), and $T = 1.3$ (high temperature), which corresponds to approximately 40, 56, and 145% of the temperature at which the athermal shear modulus of the underlying inherent states saturates.[1] For each temperature,

———

[1]In the units of the model presented in [41], this corresponds approximately to $T = 0.06$, 0.083, and 0.22.

TABLE II. High-parent-temperature athermal shear modulus and mass density for the models employed in this paper.

	2D IPL	3D IPL	4D IPL	3D POLY
$G(T_{\rm p} = \infty)$	15.8	12.4	10.9	9.22
ρ	0.86	0.82	0.80	0.65

we create 10 K samples of $N = 2000$, and 1 K samples of $N = 8000$.

All quantities in this paper are reported in dimensionless microscopic units: lengths are rescaled by $a_0 \equiv (V/N)^{1/\bar{d}}$, and times (frequencies) are rescaled by $\tau_0 \equiv a_0/c_{\rm T}$ ($\omega_0 \equiv c_{\rm T}/a_0$), where $c_{\rm T} = \sqrt{G(T_{\rm p} = \infty)/\rho}$ denotes the transverse wave speed, $G(T_{\rm p} = \infty)$ denotes the saturated (high-parent-temperature) athermal shear modulus [40], and ρ denotes the mass density. The values of ρ and $G(T_{\rm p} = \infty)$ for each model are reported in Table II.

III. THEORETICAL FRAMEWORK

We consider a disordered system of N particles in $\bar{d}$ spatial dimensions, enclosed in a fixed volume $V \equiv L^{\bar{d}}$, and interacting via a potential $U(\boldsymbol{x})$, where $\boldsymbol{x}$ denotes the $N\bar{d}$-dimensional vector of all particles' coordinates. We assume all particle masses to be unity. For all analyses, we study the system in the zero-temperature limit, meaning that it resides in a local minimum $\boldsymbol{x}_0$ of the potential energy (also called an inherent state), so that all particles are in mechanical equilibrium—the net force on each particle is zero.

In a conventional normal mode analysis, one expands the potential energy to second order in the displacement $\boldsymbol{z} \equiv \boldsymbol{x} - \boldsymbol{x}_0$ from this reference state as

$$U(\boldsymbol{x}) - U(\boldsymbol{x}_0) \simeq \tfrac{1}{2}\boldsymbol{\mathcal{M}} : \boldsymbol{zz}, \qquad (1)$$

where

$$\boldsymbol{\mathcal{M}} \equiv \frac{\partial^2 U}{\partial \boldsymbol{x} \partial \boldsymbol{x}}\bigg|_{\boldsymbol{x}_0} \qquad (2)$$

is the Hessian matrix of the potential U. Conventionally, the $N\bar{d}$ eigenvectors $\hat{\boldsymbol{\psi}}_\ell$ of $\boldsymbol{\mathcal{M}}$ are referred to as *normal modes* (also as *vibrational modes* or *harmonic modes*), with real eigenvalues $\omega_\ell^2 \geqslant 0$ (because $\boldsymbol{x}_0$ represents a local minimum of U). The eigenvectors $\hat{\boldsymbol{\psi}}_\ell$ represent orthogonal displacement directions along which the system can perform harmonic oscillatory motion with frequency ω_ℓ.

As mentioned above, structural glasses are known to feature soft quasilocalized excitations, which are displacement fields that consist of a localized, disordered core dressed by an algebraically decaying field away from the core [14]. These excitations may be approximately realized as normal modes if there exist no other modes with similar frequency in the system. However, as soon as this is no longer the case, quasilocalized excitations are manifested as *hybridized* normal modes, that mix a quasilocalized excitation with phonons or with other quasilocalized excitations, as demonstrated in Fig. 1, and discussed at length in [14] and further below. Hybridization in the normal mode analysis can be understood as a direct consequence of the orthogonalization constraint on

eigenmodes $\hat{\boldsymbol{\psi}}_\ell$: quasilocalized excitations are *not* perfectly orthogonal to phonons or other quasilocalized excitations, meaning that both phonons and quasilocalized excitations cannot be exact eigenmodes of the Hessian matrix, but must always be, to some extent, hybridized with each other.

Nonlinear quasilocalized excitations

We now present an alternative way to define quasilocalized excitations *outside* of the conventional harmonic analysis of the potential energy. Consider a glass at zero temperature and at mechanical equilibrium, the particles of which are subjected to an imposed displacement about the mechanical equilibrium state, of the form $\delta \boldsymbol{x} = s\hat{\boldsymbol{z}}$, i.e., particles are displaced a distance s in a general direction $\hat{\boldsymbol{z}}$ on the multidimensional potential-energy landscape. Since the initial state considered was a state of mechanical equilibrium, the system will respond to an imposed displacement with a restoring force, denoted here by $\boldsymbol{f}_{\hat{z}}(s)$. A third-order Taylor expansion of this force is written as

$$\boldsymbol{f}_{\hat{z}}(s) \simeq \boldsymbol{f}_1(\hat{z})s + \boldsymbol{f}_2(\hat{z})s^2 + \boldsymbol{f}_3(\hat{z})s^3, \qquad (3)$$

where the coefficients of the expansion are given by

$$\boldsymbol{f}_1(\hat{z}) = -\frac{\partial^2 U}{\partial \boldsymbol{x} \partial \boldsymbol{x}} \cdot \hat{z} = -\boldsymbol{\mathcal{M}} \cdot \hat{z}, \qquad (4)$$

$$\boldsymbol{f}_2(\hat{z}) = -\frac{1}{2}\frac{\partial^3 U}{\partial \boldsymbol{x} \partial \boldsymbol{x} \partial \boldsymbol{x}} : \hat{z}\hat{z} \equiv -\frac{1}{2}\boldsymbol{U}^{(3)} : \hat{z}\hat{z}, \qquad (5)$$

$$\boldsymbol{f}_3(\hat{z}) = -\frac{1}{6}\frac{\partial^4 U}{\partial \boldsymbol{x} \partial \boldsymbol{x} \partial \boldsymbol{x} \partial \boldsymbol{x}} : \hat{z}\hat{z}\hat{z} \equiv -\frac{1}{6}\boldsymbol{U}^{(4)} : \hat{z}\hat{z}\hat{z}. \qquad (6)$$

Once the expansion of the force response $\boldsymbol{f}_{\hat{z}}(s)$ is spelled out, a mechanical interpretation of the definition of normal modes emerges; normal modes are collective displacement directions $\hat{\boldsymbol{\psi}}$ for which $\boldsymbol{f}_1(\hat{\boldsymbol{\psi}}) \propto -\hat{\boldsymbol{\psi}}$, i.e., they are directions $\hat{\boldsymbol{\psi}}$ for which the linear force response $\boldsymbol{f}_1(\hat{\boldsymbol{\psi}})$ is *parallel* to $-\hat{\boldsymbol{\psi}}$ itself, implying that

$$\boldsymbol{\mathcal{M}} \cdot \hat{\boldsymbol{\psi}} = c_2\hat{\boldsymbol{\psi}}, \qquad (7)$$

with c_2 a scalar, for which by definition we must have $c_2 = \omega^2$. The subscript "2" refers to the fact that the modes $\hat{\boldsymbol{\psi}}$ arise from a harmonic, i.e., second-order expansion of the potential energy, in analogy with what follows.

What do we find if we instead consider collective displacement directions $\hat{\boldsymbol{\pi}}_4$ the linear force response $\boldsymbol{f}_1(\hat{\boldsymbol{\pi}}_4)$ of which is parallel to the *third-order* force response $\boldsymbol{f}_3(\hat{\boldsymbol{\pi}}_4)$, i.e., $\boldsymbol{f}_1(\hat{\boldsymbol{\pi}}_4) \propto \boldsymbol{f}_3(\hat{\boldsymbol{\pi}}_4)$? This would imply

$$\boldsymbol{\mathcal{M}} \cdot \hat{\boldsymbol{\pi}}_4 = c_4 \boldsymbol{U}^{(4)} : \hat{\boldsymbol{\pi}}_4\hat{\boldsymbol{\pi}}_4\hat{\boldsymbol{\pi}}_4. \qquad (8)$$

We coin these displacement directions $\hat{\boldsymbol{\pi}}_4$ *quartic modes*, because they arise from a fourth-order expansion of the potential energy.[2] By contracting both sides of Eq. (8) with $\hat{\boldsymbol{\pi}}_4$, the proportionality constant c_4 is found to be

$$c_4 = \frac{\kappa(\hat{\boldsymbol{\pi}}_4)}{\chi(\hat{\boldsymbol{\pi}}_4)}, \qquad (9)$$

___

[2]A similar equation for *cubic modes* may be derived by requiring $\boldsymbol{f}_2(\hat{\boldsymbol{\pi}}_3) \propto \boldsymbol{f}_1(\hat{\boldsymbol{\pi}}_3)$. We will discuss cubic modes extensively in Sec. V of this paper.
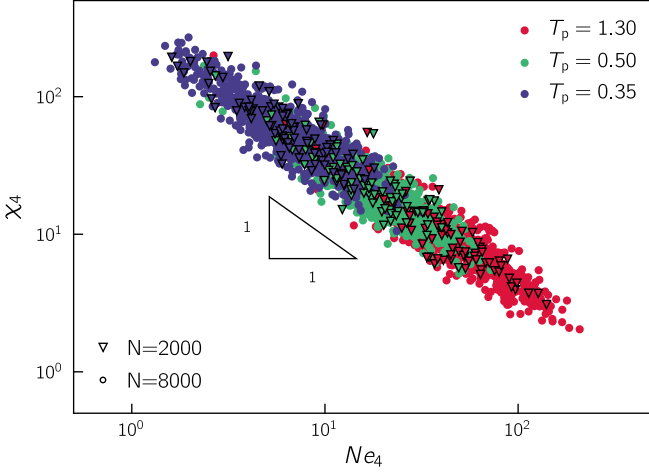
FIG. 2. The quartic expansion coefficients χ_4 are primarily sensitive to the localization Ne_4 of the associated NQEs, independent of preparation protocol or system size of the glass.

where we have defined the quartic expansion coefficient

$$\chi(z) \equiv \frac{U^{(4)} :: zzzz}{(z \cdot z)^2}, \tag{10}$$

and the stiffness κ associated with a mode z as

$$\kappa(z) \equiv \frac{\mathcal{M} : zz}{z \cdot z}. \tag{11}$$

We note that for harmonic modes $\hat{\psi}_\ell$ the stiffness $\kappa(\hat{\psi}_\ell) = \omega_\ell^2$.

We next assert that solutions $\hat{\pi}_4$ to Eq. (8), are, in fact, quasilocalized excitations. To see this, consider the energy defined as[3]

$$\mathcal{E}_4(z) = \kappa(z)^2 / \chi(z), \tag{12}$$

which is a function of a displacement field z; local minima of this energy are precisely quartic modes $\hat{\pi}_4$ by virtue of Eq. (8), namely,[4]

$$\left. \frac{\partial \mathcal{E}_4}{\partial z} \right|_{z=\hat{\pi}_4} = \mathbf{0}. \tag{13}$$

The energy function $\mathcal{E}_4$ has no straightforward physical interpretation; nevertheless, local minima of $\mathcal{E}_4$ are soft, quasilocalized excitations, since they tend to have (i) a small stiffness κ (because it appears in the enumerator) and (ii) a large quartic expansion coefficient χ (because it appears in the denominator), which, as we show now, means the mode is localized.

---

[3]In [14], the square of the energy $\mathcal{E}_4$ was called the "cost function" $\mathcal{G}_4$.

[4]Because $\mathcal{E}_4$ does not depend on the vector norm of its argument—in consistence with the fact that modes z represent *directions* in the potential-energy landscape—we can properly take the partial derivative with respect to each component of z.
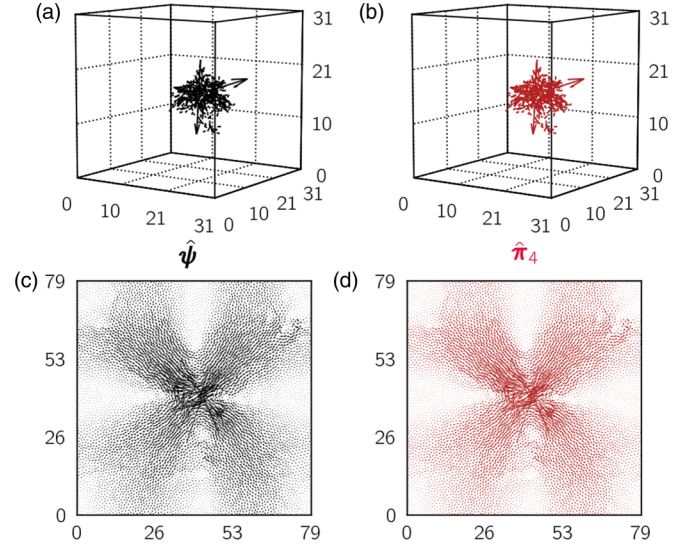

FIG. 3. Harmonic QLM $\hat{\psi}$ and quartic NQE $\hat{\pi}_4$ converge energetically and structurally in the limit of low frequencies. Panels (a) and (c) show the softest harmonic QLM in the entire ensemble of solids of the IPL model in 3D and 2D. Panels (b) and (d) show their quartic nonlinear counterparts. The relative difference in energy between the harmonic and quartic excitations $(\omega_4^2 - \omega_2^2)/\omega_4^2$ is 0.15% in 3D and 2.1% in 2D; the structural difference $1 - |\hat{\psi} \cdot \hat{\pi}_4|$ is 3.6×10^{-6} in 3D and 2.4×10^{-4} in 2D.

To demonstrate how $\chi(\hat{\pi}_4)$ is correlated with the localization of $\hat{\pi}_4$, we scatter plot in Fig. 2 $\chi_4 \equiv \chi(\hat{\pi}_4)$ vs Ne_4 [with $e_4 \equiv e(\hat{\pi}_4)$], where the participation ratio e is defined as

$$e(z) \equiv \frac{\left(\sum_i z_i \cdot z_i \right)^2}{N \sum_i (z_i \cdot z_i)^2}. \tag{14}$$

Here, z_i denotes the $\bar{d}$-dimensional coordinate vector of the ith particle. The participation ratio of a field is a measure of its degree of localization: delocalized, extended modes feature $e \sim O(1)$, whereas localized modes feature $e \sim O(1/N)$. We find that $\chi_4 \sim (Ne_4)^{-1}$, as has also been shown in [14]. Remarkably, χ_4 appears to be only sensitive to the degree of localization of $\hat{\pi}_4$, and is completely blind to the degree of annealing of the glass in which $\hat{\pi}_4$ is embedded. We present a rationalization for this general scaling relation in Appendix C.

The formulation of quartic modes, or *quartic NQEs*, as local minima of an energy $\mathcal{E}_4$, allows for their numerical computation with standard minimization methods, as described in detail in [14] and in Appendix B of this paper.

IV. NQEs ARE TRUE REPRESENTATIVES OF SOFT SPOTS

We will now establish that the NQEs defined in the previous section are true representatives of soft spots in model structural glasses. We show that NQEs do not hybridize with other low-energy excitations, and maintain their universal structure—a disordered core dressed by an algebraically
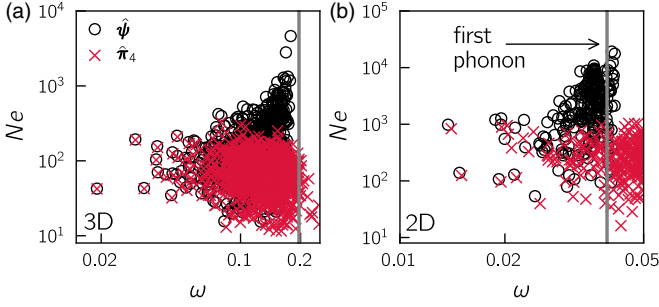
FIG. 4. Every harmonic QLM $\hat{\psi}$ has a corresponding quartic NQE $\hat{\pi}_4$ of similar frequency and participation in 3D (a) and 2D (b). Because the harmonic QLM represents the direction of lowest stiffness in the entire system, the frequency of the NQE is always slightly higher, whereas the NQE—which is free of hybridization—has a slightly lower participation ratio. When the QLM's frequency approaches the frequency of the first phonon band, hybridization becomes stronger. This is reflected in a higher participation Ne [and see also Fig. 1(c)].

decaying far field.[5] The central piece of evidence supporting our claim is the fact that in the limit $\omega \to 0$—in the absence of hybridization—harmonic QLMs converge to their corresponding NQEs both energetically and structurally. In this section, we quantitatively explain the observed convergence behavior as a consequence of normal mode hybridization. A description of our protocol for finding the lowest harmonic QLM and NQE for each system is given in Appendix B.

We first visually demonstrate the convergence of harmonic QLMs and NQEs in Fig. 3, by comparing side by side the lowest-frequency quartic NQE of our entire ensemble of solids, together with its harmonic counterpart. We confirm that when hybridization is weak the harmonic and quartic modes are nearly indistinguishable. In Fig. 4, we show that this holds for our entire ensemble of solids: every harmonic QLM has a nonlinear counterpart of very similar frequency and participation. In fact, because a harmonic QLM (below the first phonon band) by definition represents the direction of lowest energy of the system, the corresponding NQE always has a slightly *higher* energy, and—because it is not hybridized—a *lower* participation ratio. Figures 5(a) and 5(e) show that in the limit $\omega \to 0$ the relative difference in energy of these excitations scales as

$$\left(\omega_4^2 - \omega_2^2\right)/\omega_4^2 \sim f(L)\omega_4^2, \tag{15}$$

in both 2D and 3D. Here, ω_2 and ω_4 denote the frequency of the harmonic and quartic excitations, respectively. We use the notation $\omega_4 \equiv \sqrt{\kappa(\hat{\pi}_4)}$ even though, strictly speaking, ω_4 is not a vibrational frequency. $f(L)$ captures the L dependence of the prefactor, which will be discussed further below; it increases weakly with L in 3D, but strongly with L in 2D.

---

[5]We note that it may be possible to design other cost functions that—similar in spirit to $\mathcal{E}_4$ in Eq. (12)—simultaneously minimize stiffness and maximize localization, and the solutions of which also disentangle quasilocalized excitations from other low-energy excitations (see discussion in Appendix C). We will not focus on this possibility in the present paper.

Figures 5(b) and 5(f) show that the structural convergence of the QLMs and NQEs—measured by the difference of their overlaps from unity—scales as

$$1 - |\hat{\pi}_4 \cdot \hat{\psi}| \sim g(L)\omega_4^4, \tag{16}$$

in 2D and 3D, where $g(L)$ again captures the L dependence.

The ω_4 dependence of the relations Eqs. (15) and (16) was shown in [14], but no interpretation was given. In the following section, we quantitatively explain these scaling relations—including their L dependence—as a consequence of harmonic QLMs' residual hybridization, even at very small frequencies, with other low-energy excitations in the system. We thus demonstrate that NQEs are *true* quasilocalized soft spots, whereas harmonic QLMs in favorable circumstances approximate the NQEs, but are always to some degree "polluted" by other excitations due to the orthogonalization constraint of normal modes.

Scaling argument for the convergence of QLMs and NQEs

In this section, we present an argument quantitatively explaining the observed scaling relations Eqs. (15) and (16). Crucial to the discussion is the fact that any two nondegenerate normal modes must by definition be orthogonal, $\hat{\psi}_i \cdot \hat{\psi}_j = 0$. At low frequencies, excitations in the glass are either phonons or quasilocalized; an unhybridized quasilocalized excitation, which consists of a disordered core with an algebraically decaying far field, is *not* perfectly orthogonal to a phononic excitation or to other quasilocalized excitations. We conclude that in the normal mode analysis both quasilocalized excitations and phonons cannot be perfectly represented, but must always be, to however small an extent, hybridized with each other.

For the analysis that follows, we assume the lowest harmonic mode of the system is a QLM, and its vibrational frequency is significantly lower than all other frequencies of the system, so that hybridization with other modes is weak. The central observable that we use to quantify the convergence of the harmonic QLM to its nonlinear counterpart is the difference vector $\mathbf{\Delta} \equiv \hat{\pi}_4 - \hat{\psi}$, which to first order in $|\mathbf{\Delta}|$ is given by

$$\mathbf{\Delta} \simeq \omega_4^2 \sum_\ell \frac{\hat{\psi}_\ell \otimes \hat{\psi}_\ell}{\omega_\ell^2 - \omega_2^2} \left(\frac{U^{(4)} \vdots \hat{\pi}_4 \hat{\pi}_4 \hat{\pi}_4}{\chi_4} - \hat{\pi}_4 \right), \tag{17}$$

where the sum runs over all normal modes $\hat{\psi}_\ell$ *except* the lowest harmonic QLM $\hat{\psi}$. We derive this expression in Appendix D. Since the magnitude of the field $(U^{(4)} \vdots \hat{\pi}_4 \hat{\pi}_4 \hat{\pi}_4)/\chi_4$ is $O(1)$, independent of ω_4 [see Fig. 9(a) in Appendix E], and the difference $\omega_\ell^2 - \omega_2^2$ is always large by assumption, it follows from this result that

$$|\mathbf{\Delta}| \sim \omega_4^2. \tag{18}$$

1. Structural convergence

We now focus on the structural convergence of the harmonic QLM $\hat{\psi}$ to the quartic NQE $\hat{\pi}_4$. Using Eq. (18), we
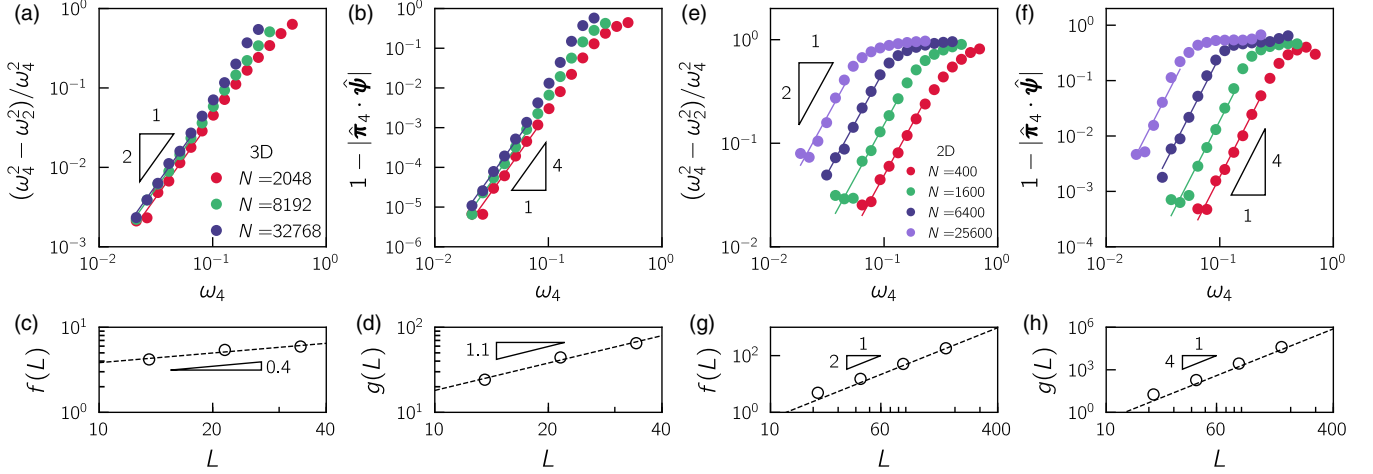
FIG. 5. Harmonic QLM $\hat{\boldsymbol{\psi}}$ and quartic NQE $\hat{\boldsymbol{\pi}}_4$ converge energetically and structurally in the limit of low frequencies. Panels (a) and (e) show the energetic convergence [Eq. (15)] in 3D and 2D. Panels (b) and (f) show the structural convergence [Eq. (16)] in 3D and 2D. Panels (c) and (d) show that the prefactors $f(L)$ and $g(L)$ of the energetic and structural convergence are weakly L dependent in 3D, whereas panels (g) and (h) show they follow $f(L) \sim L^2$ and $g(L) \sim L^4$ in 2D. For panels (a), (b), (e), and (f), the data points represent the running median.

write

$$\frac{\boldsymbol{\Delta} \cdot \boldsymbol{\Delta}}{2} = 1 - \hat{\boldsymbol{\pi}}_4 \cdot \hat{\boldsymbol{\psi}} \sim \omega_4^4, \qquad (19)$$

which gives the correct ω_4 dependence of the empirically observed Eq. (16). How can the L dependence of the prefactor $g(L)$ be understood? In Figs. 5(h) and 5(d), we show that

$$g(L) \sim L^4 \qquad (20)$$

in 2D, whereas the dependence on L is much weaker in 3D. To gain intuition for why the L dependence is so strongly dimension dependent, we visualize in Fig. 6 representative fields $\boldsymbol{\Delta}$ in 2D and 3D. $\boldsymbol{\Delta}$ always contains the disordered core of the soft quasilocalized excitation; however, it is precisely the far field of $\boldsymbol{\Delta}$ that contains physically interesting information, as it reveals which excitations are hybridized with the harmonic QLM. In 2D, the concentration of QLMs below the lowest
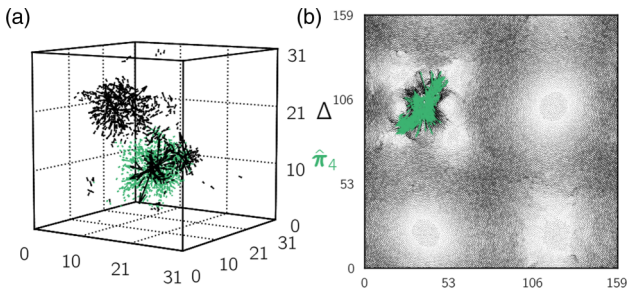

FIG. 6. Representative examples of fields $\boldsymbol{\Delta} \equiv \hat{\boldsymbol{\pi}}_4 - \hat{\boldsymbol{\psi}}$ [see Eq. (17) and discussion in text] in (a) 3D and (b) 2D are shown in black. Shown in green are the corresponding NQEs $\hat{\boldsymbol{\pi}}_4$. The magnitude of $\boldsymbol{\Delta}$ is much smaller than 1, so for visual purposes it has been scaled so that the size of the largest component of the core of $\boldsymbol{\Delta}$ matches the corresponding component of $\hat{\boldsymbol{\pi}}_4$. For visualization purposes, we show only the largest 2% of components of $\boldsymbol{\Delta}$ and $\hat{\boldsymbol{\pi}}_4$ in 3D, and the largest 1.4% of $\hat{\boldsymbol{\pi}}_4$ in 2D.

phonon band is lower than in 3D,[6] and therefore the hybridization with the lowest QLM is dominated by the phonons in the first phonon band, as the field $\boldsymbol{\Delta}$ in Fig. 6(b) clearly shows. This implies that the sum in Eq. (17) is dominated by the first phonon band, the frequency of which scales as $\omega_{\mathrm{ph}} \sim L^{-1}$, from which it follows that $1/(\omega_{\mathrm{ph}}^2 - \omega_2^2) \sim L^2$. Hence,

$$\boldsymbol{\Delta} \sim \omega_4^2 L^2 [\hat{\boldsymbol{\psi}}_{\mathrm{ph}} \cdot (\boldsymbol{U}^{(4)} \vdots \hat{\boldsymbol{\pi}}_4 \hat{\boldsymbol{\pi}}_4 \hat{\boldsymbol{\pi}}_4 / \chi_4 - \hat{\boldsymbol{\pi}}_4)] \hat{\boldsymbol{\psi}}_{\mathrm{ph}}. \qquad (21)$$

To obtain the full L dependence of $\boldsymbol{\Delta}$, we next consider the overlap $\hat{\boldsymbol{\psi}}_{\mathrm{ph}} \cdot (\boldsymbol{U}^{(4)} \vdots \hat{\boldsymbol{\pi}}_4 \hat{\boldsymbol{\pi}}_4 \hat{\boldsymbol{\pi}}_4 / \chi_4 - \hat{\boldsymbol{\pi}}_4)$. The triple contraction $(\boldsymbol{U}^{(4)} \vdots \hat{\boldsymbol{\pi}}_4 \hat{\boldsymbol{\pi}}_4 \hat{\boldsymbol{\pi}}_4) / \chi_4$ decays as $r^{-3\bar{d}}$ away from the core of the NQE [14], and so its overlap with a phonon—an extended field—is small. The overlap with $\hat{\boldsymbol{\pi}}_4$, which has a far-field decay of $r^{1-\bar{d}}$, therefore dominates. Furthermore, the decay $r^{1-\bar{d}}$ implies that—because the surface of a sphere in $\bar{d}$ dimensions scales as $r^{\bar{d}-1}$—the contraction of $\hat{\boldsymbol{\pi}}_4$ with an extended field is system-size independent. These considerations together lead to the prediction that, if hybridization is due to the lowest phonons, $|\boldsymbol{\Delta}| \sim L^2 \omega_4^2$. Together with Eq. (19) this explains Eq. (20), and we conclude that in 2D hybridization is indeed dominated by the lowest phonons.

Turning to the 3D case, we observe that typical fields $\boldsymbol{\Delta}$ are *not* wavelike, but instead mainly feature other QLMs in the far field, as shown in Fig. 6(a). This means that the sum in Eq. (17) is dominated by other QLMs *below* the lowest phonon band. In the overlap between these QLMs and the field $(\boldsymbol{U}^{(4)} \vdots \hat{\boldsymbol{\pi}}_4 \hat{\boldsymbol{\pi}}_4 \hat{\boldsymbol{\pi}}_4 / \chi_4 - \hat{\boldsymbol{\pi}}_4)$, the term $\hat{\boldsymbol{\pi}}_4$ again dominates. $\hat{\boldsymbol{\pi}}_4$ couples only to QLMs in the vicinity, since these objects

---

[6]Since QLMs' frequencies are independently distributed according to $\mathcal{D}(\omega) \sim \omega^4$, a Weibullian scaling argument predicts that the frequency of the lowest QLM in a system of linear size L follows $\langle \omega_{\min} \rangle (L) \sim L^{-d/5}$ [13]. The lowest phonon frequency scales as L^{-1}, independent of dimension, explaining why—all else being equal—QLMs fall below the lowest phonon band less frequently in 2D than in 3D.

decay as r^{1-d} from their core; the frequency difference between the lowest QLM with the second lowest, third lowest, etc., with non-negligible overlap is therefore only weakly dependent on L.[7] Consequently, we expect $g(L)$ to be weakly L dependent also, as we indeed observe.

2. Energetic convergence

Finally, we focus on the energetic convergence between the harmonic QLM $\hat{\boldsymbol{\psi}}$ and the corresponding NQE $\hat{\boldsymbol{\pi}}_4$, given by Eq. (15). The energy of $\hat{\boldsymbol{\pi}}_4 = \hat{\boldsymbol{\psi}} + \boldsymbol{\Delta}$ is written as

$$\omega_4^2 \equiv \mathcal{M} : \hat{\boldsymbol{\pi}}_4 \hat{\boldsymbol{\pi}}_4 = \omega_2^2 + \mathcal{M} : \boldsymbol{\Delta}\boldsymbol{\Delta} + 2\mathcal{M} : \hat{\boldsymbol{\psi}}\boldsymbol{\Delta}. \quad (22)$$

To rewrite the third term, we use the fact that $\mathcal{M} \cdot \hat{\boldsymbol{\psi}} = \omega_2^2 \hat{\boldsymbol{\psi}}$, and the result from the previous discussion $\hat{\boldsymbol{\psi}} \cdot \boldsymbol{\Delta} = -|\boldsymbol{\Delta}|^2/2$ [see Eq. (19)]. After rearranging, we obtain

$$\omega_4^2 - \omega_2^2 = |\boldsymbol{\Delta}|^2 \mathcal{M} : \hat{\boldsymbol{\Delta}}\hat{\boldsymbol{\Delta}} - |\boldsymbol{\Delta}|^3 \omega_2^2. \quad (23)$$

$\mathcal{M} : \hat{\boldsymbol{\Delta}}\hat{\boldsymbol{\Delta}}$ represents the typical stiffness of the hybridized excitations, which by assumption is much larger than ω_2^2. We can thus safely neglect the $O(|\boldsymbol{\Delta}|^3)$ term. As we discussed above, $|\boldsymbol{\Delta}|$ scales inversely proportionally to the stiffness of the typical harmonic modes that hybridize with the lowest QLM, owing to the factor $(\omega_\ell^2 - \omega_2^2)^{-1} \sim (\mathcal{M} : \hat{\boldsymbol{\Delta}}\hat{\boldsymbol{\Delta}})^{-1}$ in the sum in Eq. (17). Using Eq. (18), we obtain

$$\frac{\omega_4^2 - \omega_2^2}{\omega_4^2} \sim \frac{\omega_4^2}{\mathcal{M} : \hat{\boldsymbol{\Delta}}\hat{\boldsymbol{\Delta}}}. \quad (24)$$

In 2D, where hybridization is dominated by the lowest phonons, $\mathcal{M} : \hat{\boldsymbol{\Delta}}\hat{\boldsymbol{\Delta}} \sim \omega_{\text{ph}}^2 \sim L^{-2}$, so that

$$f(L) \sim L^2, \quad (25)$$

which is validated numerically in Fig. 5(g). In 3D, hybridization is dominated by nearby QLMs below the lowest phonon band, so that $f(L)$ scales weakly with L (see footnote 7). This is validated in Fig. 5(c).

In conclusion, we have quantitatively predicted the convergence of harmonic QLMs to their quartic counterparts as a consequence of the unavoidable hybridization of harmonic modes—with phonons and/or other QLMs of similar frequencies—strongly reinforcing our claim that quartic NQEs are true representatives of quasilocalized soft excitations in glasses.

V. NQEs REVEAL UNIVERSAL PROPERTIES OF THE POTENTIAL-ENERGY LANDSCAPE

In the previous sections we focused on NQEs that are represented by solutions $\hat{\boldsymbol{\pi}}_4$ to Eq. (8), referred to as quartic modes. In Sec. III, quartic modes were defined as displacement directions for which the linear force response is parallel to the third-order force response, $\boldsymbol{f}_1(\hat{\boldsymbol{\pi}}_4) \propto \boldsymbol{f}_3(\hat{\boldsymbol{\pi}}_4)$. However,

---

[7] The scaling argument discussed in footnote 6 also applies to the second-lowest, third-lowest, etc., frequency. Since QLMs have non-negligible overlap only with other QLMs in their vicinity, the frequency difference between the lowest QLM and the next lowest in its vicinity is expected to depend very weakly on L.

another important class of NQEs is that of displacement directions $\hat{\boldsymbol{\pi}}_3$ for which the linear force response is parallel to the *second-order* force response, $\boldsymbol{f}_1(\hat{\boldsymbol{\pi}}_3) \propto \boldsymbol{f}_2(\hat{\boldsymbol{\pi}}_3)$. Analogously to Eq. (8), this implies

$$\mathcal{M} \cdot \hat{\boldsymbol{\pi}}_3 = c_3 \boldsymbol{U}^{(3)} : \hat{\boldsymbol{\pi}}_3 \hat{\boldsymbol{\pi}}_3. \quad (26)$$

We refer to these modes as *cubic modes*, because their definition requires a third-order expansion of the potential energy. By contracting both sides of Eq. (26) with $\hat{\boldsymbol{\pi}}_3$, we find

$$c_3 = \frac{\kappa(\hat{\boldsymbol{\pi}}_3)}{\tau(\hat{\boldsymbol{\pi}}_3)}, \quad (27)$$

where we have defined the cubic expansion coefficient:

$$\tau(z) \equiv \frac{\boldsymbol{U}^{(3)} \vdots zzz}{(z \cdot z)^{3/2}}. \quad (28)$$

Cubic modes were first introduced in [30], where they were shown to be very accurate representatives of the loci and geometry of imminent plastic instabilities that occur in sheared athermal glasses. In addition, the stiffnesses $\kappa_3 \equiv \kappa(\hat{\boldsymbol{\pi}}_3)$ associated with cubic modes were shown to follow a simple dynamics with imposed shear strain γ, namely [24],

$$\frac{d\kappa_3}{d\gamma} \simeq -\frac{\tau_3 \nu_3}{\kappa_3}, \quad (29)$$

which becomes exact in the limit of small κ_3. Here $\nu_3 \equiv \frac{\partial^2 U}{\partial\gamma\partial\boldsymbol{x}} \cdot \hat{\boldsymbol{\pi}}_3$ is the shear-strain-coupling parameter associated with the cubic mode $\hat{\boldsymbol{\pi}}_3$. These properties of cubic modes suggest that they are promising candidates to represent the shear transformation zones envisioned by Falk and Langer in their seminal work on plastic deformation in glasses [45], as discussed in detail in [24].

In this section we first discuss the energetic and statistical properties of cubic modes, and explain their differences and similarities compared to quartic modes. To this end, we study an ensemble of pairs of cubic and quartic modes that represent the *same* soft spot in each of our computer glasses. The details of these calculations are presented in Appendix B. Finally, based on the unique mechanical properties of cubic modes, we make predictions about the universal statistical properties of generic computer glasses' potential-energy landscape, and about their destabilization under shear.

A. Cubic modes' energetics

In Fig. 7(a) we plot the relative increase of cubic modes' stiffnesses ω_3^2 over quartic modes' stiffnesses ω_4^2 (in our data, cubic modes' stiffnesses are larger than quartic modes' stiffnesses in over 99.5% of cases). We find that cubic modes' stiffnesses are typically approximately 30% higher than those of quartic modes that represent the same soft spots (corresponding to frequencies that are typically 14% higher), independent of the frequency associated with those soft spots. In other words, we find that the *relative* increase in frequency of cubic modes compared to quartic modes is constant, and independent of frequency. Since the distribution of quartic modes is expected to follow $\mathcal{D}(\omega_4) \sim \omega_4^4$ for small frequencies—owing to their convergence to harmonic modes,
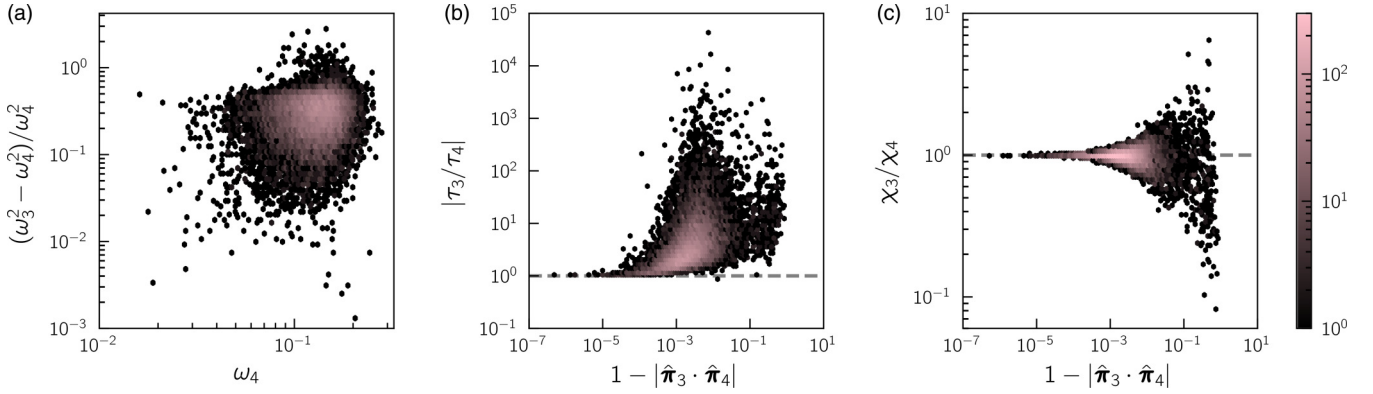
FIG. 7. Difference between cubic and quartic NQEs. Panel (a) shows that the relative energy difference between cubic and quartic modes is approximately 30%, independent of frequency, corresponding to a relative frequency difference of about 14%. Panel (b) shows that the third-order coefficients τ_3 and τ_4, which are a measure of the asymmetry of the energy landscape along the mode, are highly sensitive to the modes' structure, as quantified by the difference from unity of their overlap, $1 - |\hat{\boldsymbol{\pi}}_3 \cdot \hat{\boldsymbol{\pi}}_4|$. Panel (c) shows that the fourth-order coefficients χ_3 and χ_4 are insensitive to small changes in the modes' structure, consistent with the fact that χ scales inversely with the participation ratio (see Fig. 2), which is a global geometric measure. We emphasize that in panel (b) the data span almost five orders of magnitude, whereas in panel (c) the data span less than one. All data are reported as 2D histograms, with the bin counts given by the color of the bin.

which feature $\mathcal{D}(\omega_2) \sim \omega_2^4$ in the absence of strong hybridization [13,16,18,19,38]—this means that the distribution of cubic modes is also expected to follow

$$\mathcal{D}(\omega_3) \sim \omega_3^4 \quad \text{as} \quad \omega_3 \to 0, \tag{30}$$

which will be key to additional results derived in what follows.

In order to understand why the frequency of a cubic mode is generally higher than that of the quartic mode that represents the same soft spot, we plot in Fig. 7(b) the absolute magnitude of the ratio of the third-order coefficients associated with cubic modes, to the third-order coefficients associated with quartic modes, $|\tau_3/\tau_4|$, against the difference from unity of their overlap $1 - |\hat{\boldsymbol{\pi}}_3 \cdot \hat{\boldsymbol{\pi}}_4|$. These data indicate that very minute differences in the modes' structure can lead to very large—up to several orders of magnitude—changes in their third-order coefficients.

In contrast, the data presented in Fig. 7(c) indicate that fourth-order coefficients χ_3 and χ_4 are quite indifferent to small changes in modes' structure. This is expected, since we demonstrated in Fig. 2 that fourth-order coefficients are primarily sensitive to the degree of localization of their associated modes, which is a purely geometric measure. As discussed in Sec. III, quartic modes are defined by collective displacements that feature both small stiffnesses $\kappa_4 \equiv \omega_4^2$ *and* large fourth-order coefficients χ_4, as can be deduced from the "quartic energy" function [Eq. (12)], of which modes $\hat{\boldsymbol{\pi}}_4$ are local minima. Having established that the coefficients χ_4 associated with quartic modes are insensitive to details in the mode's structure, we conclude that maximizing χ_4 does not impose large constraints on minimizing ω_4.

For cubic modes, a similar "cubic energy" is given by[8]

$$\mathcal{E}_3(z) \equiv \frac{\kappa(z)^3}{\tau(z)^2}. \tag{31}$$

Analogously to the scenario for quartic modes, cubic modes—being local minima of $\mathcal{E}_3$—tend to have small stiffnesses κ_3, and large *third-order* coefficients τ_3. Since the coefficients τ_3 are very sensitive to fine details of cubic modes' structure, as we have shown in Fig. 7(b), we expect that maximizing τ_3 imposes large constraints on cubic modes' frequencies ω_3, which, in turn, explains why they are generally larger than quartic modes' frequencies.

B. Cubic modes' stability

Within the soft potential model [1,2], a stability argument is spelled out, according to which the expansion coefficients $\kappa, \tau,$ and χ associated with soft QLMs satisfy the soft inequality

$$\tau^2 \leqslant 3\kappa\chi, \tag{32}$$

independent of glass stability. This soft inequality implies that, within a quartic expansion of the potential energy along a soft QLM, if a second minimum exists—meaning that the expansion represents a double-well potential—the energy of the second potential well is necessarily *larger* than the minimum in which the system resides.

Based on the sensitivity of NQEs' third-order coefficients τ to the fine details of NQEs' structure, as demonstrated in the previous subsection [see Fig. 7(b)], we argue that inequality (32) can only be meaningfully tested with cubic modes, since cubic modes' third-order coefficients τ_3 are maximal, while still maintaining approximately the *same frequencies as the softest NQEs*—the quartic modes—as shown in Fig. 7(a). In other words, we assert that the third-order coefficients of quartic modes (τ_4) or of harmonic QLMs (τ_2) do *not* represent the true asymmetry of soft spots, but, crucially, that τ_3 does.

We therefore scatter plot in Fig. 8 the third-order coefficients τ_3 of cubic modes vs the product $\kappa_3\chi_3$, calculated for low-lying cubic modes in very stable (blue circles), intermediately stable (green circles), and very unstable (red circles) glasses of $N = 8000$ particles. We find that while the inequality (32) is not strictly satisfied—and less so for less
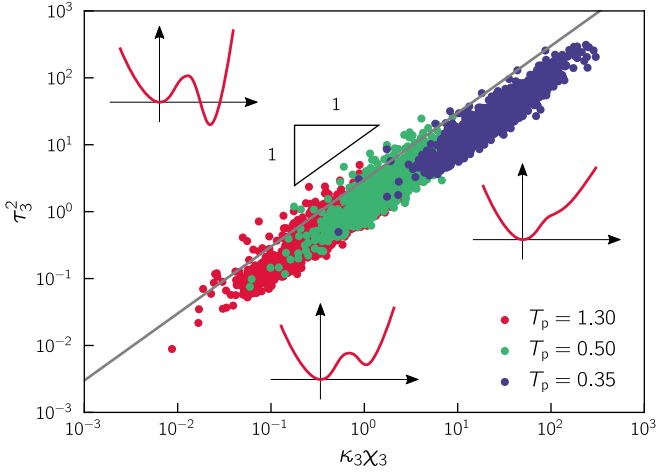
---

[8]In [14], $\mathcal{E}_3$ was called the "cost function" $\mathcal{G}_3$, and in [24,30] it was called the "barrier function" b.

FIG. 8. The ensemble of cubic modes follows $\tau_3^2 \sim \kappa_3\chi_3$, independent of glass stability. The continuous line marks the bound given by Eq. (32), at which the mode—in the fourth-order expansion of the potential energy—is a symmetric double-well potential. Modes that fall below this bound either are single-well potentials or have a second minimum that has a higher energy than the inherent state. Modes that exceed this bound have a second minimum with a lower energy than the inherent state (see illustrations). In our ensemble of solids, only 6.6% ($T_p = 1.30$), 4.6% ($T_p = 0.50$), and 0.5% ($T_p = 0.35$) of cubic modes exceed this bound. In Fig. 9(c) (in Appendix E), we demonstrate that χ_3 is independent of κ_3, which together with the data in this figure demonstrates that $\tau_3 \sim \sqrt{\kappa_3} \sim \omega_3$, which is central to the predictions that follow in the next section.

stable glasses— the *entire* set of cubic modes follows

$$\tau_3^2 \sim \kappa_3\chi_3, \tag{33}$$

independent of glass stability. This is one of the key results of this paper.

Since χ_3 is independent of frequency, as demonstrated in Fig. 9(c) in Appendix E, we conclude that cubic modes universally follow

$$\tau_3 \sim \omega_3, \tag{34}$$

independent of spatial dimension, glass preparation protocol, or microscopic details.

We demonstrate in Fig. 9(d) of Appendix E that indeed Eq. (33) holds in 2D, 3D, and 4D. Finally, we reinforce our statement that only cubic modes accurately capture the third-order coefficient of soft spots in Fig. 9(e), by demonstrating that the ensemble of quartic modes does *not* follow the relation $\tau_4^2 \sim \kappa_4\chi_4$.

C. Implications on the statistical properties of the potential-energy landscape

The universal linear scaling between τ_3 and ω_3 [see Eq. (34), Figs. 8 and 9(c), and the discussion in the preceding subsection] has two major implications, spelled out here. We focus the discussion exclusively on cubic modes, and therefore omit the subscript "3" in what follows.

1. Potential-energy barrier distribution

In the limit $\omega \to 0$, the magnitude V_B of potential-energy barriers that surround a glassy inherent state scales with the coefficients of the NQEs associated with those barriers as [30]

$$V_B \sim \kappa^3/\tau^2 \sim \omega^4, \tag{35}$$

where we have used Eq. (34). We further recall that the distribution of cubic modes' frequencies was argued in Sec. V A to follow the universal $\mathcal{D}(\omega) \sim \omega^4$ law. Combining these two statements, we obtain a prediction for the distribution of potential-energy barriers in the limit $V_B \to 0$ by a simple transformation of variables, that reads

$$p(V_B) \sim V_B^{1/4}. \tag{36}$$

The universality of Eq. (34) and of the form of $\mathcal{D}(\omega)$ implies that the distribution of potential-energy barriers should universally follow the $V_B^{1/4}$ law in any model glass, independent of dimension, microscopic details, or preparation protocol[9]—as long as the glasses considered are quenched from a melt.[10] We are currently unaware of numerical data that confirm or refute our prediction Eq. (36). We note that methods to find energy barriers between inherent states do exist [48–52], but they are computationally expensive and not exhaustive.

2. Strain intervals before the first plastic instability

Much attention has been devoted to understanding the statistics of strain intervals between subsequent plastic instabilities that occur during athermal, quasistatic deformation of computer glasses [53–62]. In particular, the distribution $p(x) \sim x^\theta$ of local relative strain thresholds x, its finite-size manifestations, and its evolution with shear strain have been recently debated [58,59].

Here we recall a result put forward in [24], that states that the additional local shear deformation x necessary to destabilize a strain-coupled cubic mode follows

$$x \sim \frac{\omega^4}{\tau\nu}, \tag{37}$$

where ν is the same shear-strain-coupling parameter associated with the NQE $\hat{\pi}$ as defined after Eq. (29). In Fig. 9(b) of Appendix E we show that the statistics of the shear-strain-coupling parameter are independent of frequency; therefore, based on Eqs. (34) and (37) we expect $x \sim \omega^3$. Together with Eq. (34) and the universal distribution $\mathcal{D}(\omega) \sim \omega^4$ of cubic modes, we predict that for as-quenched, isotropic configurations the distribution of local relative deformation thresholds should follow

$$p(x) \sim x^{2/3}, \tag{38}$$

---

[9]The assumptions leading to Eq. (36) have been validated in 2D, 3D, and 4D [see [16] for the universality of $\mathcal{D}(\omega) \sim \omega^4$, and Fig. 9(d) for the universality of Eq. (33)]. Preliminary evidence suggests that the universal form of $\mathcal{D}(\omega)$ persists in even higher dimensions [46], and we speculate that this might also be the case for Eq. (36).

[10]A counterexample are the glasses discussed in [47], which are not quenched from a melt and feature a gapped $\mathcal{D}(\omega)$, and therefore presumably also a gapped $p(V_B)$.

i.e., we predict that $\theta = 2/3$, independent of spatial dimension, microscopic details, or glass preparation protocol. We note that the mean-field theory put forward in [59] predicts $\theta = 1/2$ for as-quenched, isotropic configurations, while elastoplastic models feature $\theta \approx 0.6$ in 2D, and $\theta \approx 0.4$ in 3D [57].

The strain interval up to a first plastic instability in a system of size N is now straightforwardly predicted by assuming that it is controlled by the minimal member x_{min} out of a population of size $\propto N$ of strain thresholds x, namely (see also footnote 6),

$$x_{min} \sim N^{-\frac{1}{1+\theta}} \sim N^{-\frac{3}{5}}, \qquad (39)$$

in good agreement with [55] where a dimension-independent exponent of -0.62 was measured for the N dependence of x_{min}, and in excellent agreement with [61] where an exponent of approximately -0.6 was found for 2D computer glasses. Other numerical results in 3D feature protocol-dependent exponents ranging between 0.3 and 0.6 [63]. We note that $x_{min}(N)$ is expected to exhibit strong finite-size effects in stable glasses, because small samples do not feature enough soft quasilocalized excitations for the extreme-value scaling argument Eq. (39) to hold, as discussed at length in [61]. In addition to this, there is another independent finite-size effect that can affect the exponent θ, and therefore the scaling of $x_{min}(N)$. In [38], it was shown that when the system size is too small (smaller than the typical core size of QLMs) the density of states of quasilocalized excitations follows

$$\mathcal{D}(\omega) \sim \omega^{\beta}, \qquad (40)$$

with β slightly smaller than 4. This effect is especially noticeable in poorly quenched glasses, which possess quasilocalized excitations with relatively larger disordered cores. In this case, we predict

$$\theta = (\beta - 2)/3 \qquad (41)$$

[see Eq. (38)], and

$$x_{min} \sim N^{-3/(1+\beta)}, \qquad (42)$$

i.e., we predict a decay slightly stronger than Eq. (39) for smaller systems.

VI. DISCUSSION AND OUTLOOK

In this paper, we have shown that NQEs are true representatives of soft spots in glasses, unlike the widely used harmonic modes, that—due to their orthogonality constraint—always feature a degree of hybridization with other low-energy excitations. We have further shown that a particular class of NQEs, termed *cubic NQEs*, reveals universal properties of the potential-energy landscape, from which we derive a prediction for the distribution of the lowest energy barriers separating inherent states, and a prediction for the distribution of local strain thresholds to plastic instability.

The practical utility of the nonlinear formulation of soft spots depends crucially on whether all (or most) of the low-energy solutions to the defining equations [Eq. (8) for quartic and Eq. (26) for cubic modes] can be found. This is

a computational challenge that we will take up in future work, where we will present a method to find the vast majority of low-lying NQEs—and, hence, an approximation to the full distribution of soft spots. This will open up several avenues of research to further our understanding of fundamental problems in glass physics, such as the anomalous thermodynamic and transport properties of glasses, yielding, and dynamics in the viscous liquid regime (see citations in the Introduction), some of which will be extensively discussed in future work.

Another important future research direction is the study of the properties and statistics of NQEs near the *unjamming* transition [7,64–66]. This transition marks the loss of rigidity of the system upon decreasing the degree of connectedness (measured by the excess coordination δz) of the underlying network of strong interactions below a critical value ($\delta z = 0$), which can, for example, be achieved by decompressing a packing of repulsive soft spheres. Near this transition, the potential-energy landscape becomes highly rugged and hierarchical, and the displacement directions that connect nearby energy minima become delocalized [67,68]; in contrast, the systems studied in this paper are far from unjamming, and feature simpler energy landscapes, with localized "hopping" between energy minima [68]. We expect that NQEs will still properly represent soft harmonic QLMs near the unjamming transition. This would imply that the size of their disordered core will diverge as $1/\sqrt{\delta z}$ [69], and their characteristic frequency scale—which is expected to follow the bulk average of the frequency of the system's response to a local force dipole [19,70]—will scale as δz [71].

It is important to stress that our prediction for the distribution of local strain thresholds to a plastic instability $p(x) \sim x^{\theta}$, with $\theta = 2/3$, only holds in the *isotropic state*, i.e., shear strain $\gamma = 0$, where the relations $\tau_3 \sim \omega_3$ and $\mathcal{D}(\omega) \sim \omega^4$ hold. At finite γ the relation $\tau_3 \sim \omega_3$ must break down, because destabilizing cubic modes' third-order coefficients τ_3 were shown to remain constant upon approaching the instability strain [24], whereas their frequency vanishes. Moreover, it was recently shown that under shear $\mathcal{D}(\omega) \sim \omega^4$ does not always hold, but instead an exponent smaller than 4 is observed for well-annealed glasses [63].

This is consistent with recent numerical investigations which have highlighted a nonmonotonic behavior of θ as a function of γ. In particular, it was shown that θ first decreases as a function of γ, before increasing again upon approaching the yielding transition, and finally reaching a plateau value $\theta \approx 1/2$ in the steady state regime [55,58,63]. Furthermore, it was reported that the decrease of θ at intermediate strain is protocol dependent and is significantly stronger for better-annealed glasses [58,62]. Directly measuring the evolution of $\mathcal{D}(\omega)$ and the joint distribution $P(\omega_3, \tau_3)$ under shear, for various degrees of annealing, is therefore a highly promising direction of future research.

ACKNOWLEDGMENTS

APPENDIX A: TENSORIAL NOTATION

To aid readability, in this paper we omit particle indices (denoted here by roman letters, e.g., $i = 1, \ldots, N$) and Cartesian (spatial) indices (denoted here by greek letters, e.g., $\alpha = x, y, z$) from all tensorial and vectorial quantities. For example, the $N\bar{d}$-dimensional vector $\boldsymbol{x}$ should be understood as x_i^α, and the tensor $\boldsymbol{U}^{(4)} \equiv \frac{\partial U}{\partial \boldsymbol{x} \partial \boldsymbol{x} \partial \boldsymbol{x} \partial \boldsymbol{x}}$ should be understood as $\frac{\partial U}{\partial x_i^\alpha \partial x_j^\beta \partial x_k^\gamma \partial x_l^\delta}$. We denote single, double, triple, and quadruple contractions by $\cdot$, $:$, $\vdots$ and $::$, respectively. For example, the expression $\boldsymbol{U}^{(4)} \vdots zzz$ should be understood as $\frac{\partial U}{\partial x_i^\alpha \partial x_j^\beta \partial x_k^\gamma \partial x_l^\delta} z_i^\alpha z_j^\beta z_k^\gamma$, where the summation convention applies.

APPENDIX B: NQE ANALYSIS

For all models used, we obtain a collection of low-energy harmonic QLM and corresponding quartic and cubic modes as follows. For each system, we first find the lowest eigenvalue and eigenmode of the Hessian matrix (not including the $\bar{d}$ translational modes) using ARPACK [72]. Then, we use the lowest eigenmode as an initial vector to locally minimize the quartic energy function [Eq. (12)] to obtain the corresponding quartic NQE. Finally, we use the quartic mode as an initial vector to locally minimize the cubic energy function [Eq. (31)] to obtain the corresponding cubic mode. This procedure results in one harmonic, one quartic, and one cubic mode for each system.

For the 3D POLY model, we apply an additional procedure to find a low-energy cubic NQE in each system. Besides the quartic NQE, we consider as initial vectors the six *nonaffine velocities* [73] that result from imposing a simple and pure shear deformation in the *XY*, *XZ*, and *YZ* plane. From these seven initial guesses, we select the cubic NQE with the lowest stiffness.

To minimize the cubic and quartic energy functions, we use the MACOPT conjugate-gradient minimizer [74], modified such that the variable vector z is always kept normalized.

The two quartic modes shown in Fig. 1(b) were found as follows. The first quartic mode, shown in black, was found by using the harmonic double-core QLM $\hat{\boldsymbol{\psi}}$ [see panel (a)] as an initial condition to minimize the quartic energy function. The second quartic mode, shown in green, was found by using the difference between $\hat{\boldsymbol{\psi}}$ and the first quartic mode as an initial condition.

APPENDIX C: SCALING RELATION BETWEEN PARTICIPATION AND THE FOURTH-ORDER EXPANSION COEFFICIENT

In this Appendix we explain the scaling relation $\chi_4 \sim (Ne_4)^{-1}$, that holds independently of system size and glass preparation protocol, as shown in Fig. 2. Here, $\chi_4 \equiv \chi(\hat{\boldsymbol{\pi}}_4)$ is the fourth-order expansion coefficient [Eq. (10)], and $e_4 \equiv e(\hat{\boldsymbol{\pi}}_4)$ is the participation ratio [Eq. (14)], associated with quartic modes $\hat{\boldsymbol{\pi}}_4$.

First, observe that for any normalized mode we have

$$\frac{1}{Ne(\hat{z})} = \sum_i^N (\hat{z}_i \cdot \hat{z}_i)^2. \tag{C1}$$

We now argue that $\chi(\hat{z}) \equiv \boldsymbol{U}^{(4)} :: \hat{z}\hat{z}\hat{z}\hat{z}$ has a similar structure. For example, for radially symmetric pairwise potentials, we have

$$\chi(\hat{z}) = \sum_{\langle ij \rangle} \left(\frac{\varphi_{ij}''''}{r_{ij}^4} - \frac{6\varphi_{ij}'''}{r_{ij}^5} + \frac{15\varphi_{ij}''}{r_{ij}^6} - \frac{15\varphi_{ij}'}{r_{ij}^7} \right) (\boldsymbol{x}_{ij} \cdot \hat{z}_{ij})^4$$

$$+ 6 \sum_{\langle ij \rangle} \left(\frac{\varphi_{ij}'''}{r_{ij}^3} - \frac{3\varphi_{ij}''}{r_{ij}^4} + \frac{3\varphi_{ij}'}{r_{ij}^5} \right) (\boldsymbol{x}_{ij} \cdot \hat{z}_{ij})^2 (\hat{z}_{ij} \cdot \hat{z}_{ij})$$

$$+ 3 \sum_{\langle ij \rangle} \left(\frac{\varphi_{ij}''}{r_{ij}^2} - \frac{\varphi_{ij}'}{r_{ij}^3} \right) (\hat{z}_{ij} \cdot \hat{z}_{ij})^2, \tag{C2}$$

where the sums run over $O(N)$ interacting pairs $\langle ij \rangle$. Here, $\boldsymbol{x}_{ij} \equiv \boldsymbol{x}_j - \boldsymbol{x}_i$ and $\hat{z}_{ij} \equiv \hat{z}_j - \hat{z}_i$. Aside from prefactors and contractions with $\boldsymbol{x}_{ij}$, every term scales as $|\hat{z}_{ij}|^4$. So $\chi(\hat{z}) \sim \sum_{\langle ij \rangle} |\hat{z}_{ij}|^4$ functions rather like $1/Ne(\hat{z})$, except that $\hat{z}_i$ is replaced by $\hat{z}_{ij}$ [see Eq. (C1)], which explains the observed scaling $\chi_4 \sim (Ne_4)^{-1}$. Furthermore, it explains why quartic modes, in addition to having a low participation, so effectively disentangle localized soft spots from a phonon background: terms that scale as $|\hat{z}_{ij}|^4$ are extremely small for phononlike fields, meaning that those fields are suppressed in the minima of the associated nonlinear cost function [see Eq. (12)].[11] This suggests that minima of a cost function in which $\chi(\hat{z})$ is replaced by the purely geometric factor $\sum_{\langle ij \rangle} (\hat{z}_{ij} \cdot \hat{z}_{ij})^2$, i.e.,

$$C(z) = \frac{(\mathcal{M} : zz)^2}{\sum_{\langle ij \rangle} (z_{ij} \cdot z_{ij})^2}, \tag{C3}$$

will be similar to quartic modes.

APPENDIX D: DERIVATION OF THE EXPRESSION FOR Δ

In this Appendix, we present a derivation of Eq. (17) for the difference vector of the quartic NQE (of stiffness ω_4^2) and the harmonic QLM (of stiffness ω_2^2), denoted by $\boldsymbol{\Delta} \equiv \hat{\boldsymbol{\pi}} - \hat{\boldsymbol{\psi}}$. This derivation is very similar to the one presented in [24] for the difference between the cubic NQE and the destabilizing harmonic mode near a plastic instability under an imposed shear deformation.

Recall that the stiffness associated with a particular displacement field z is defined as

$$\kappa(z) = \frac{\mathcal{M} : zz}{z \cdot z}. \tag{D1}$$

For the analysis that follows, we require the first and second derivatives

$$\frac{\partial \kappa}{\partial z} = \frac{2}{z \cdot z}[\mathcal{M} \cdot z - \kappa(z)z], \tag{D2}$$

$$\frac{\partial^2 \kappa}{\partial z^2} = \frac{2}{(z \cdot z)^2}[(z \cdot z)\mathcal{M} - 4(\mathcal{M} \cdot z) \otimes z$$
$$- (\mathcal{M} : zz)\mathcal{I} + 4\kappa(z)z \otimes z]. \tag{D3}$$

Here, $\mathcal{I}$ denotes the identity matrix. We will now leverage the fact that the harmonic QLM represents the system's displacement direction of smallest stiffness, so that

$$\left.\frac{\partial \kappa}{\partial z}\right|_{\hat{\psi}} = 0. \tag{D4}$$

We write down the first-order Taylor expansion of the function $\frac{\partial \kappa}{\partial z}$ around $z = \hat{\psi}$ to approximate

$$\left.\frac{\partial \kappa}{\partial z}\right|_{\hat{\pi}} \simeq \left.\frac{\partial^2 \kappa}{\partial z^2}\right|_{\hat{\psi}} \cdot \Delta. \tag{D5}$$

Inverting in favor of Δ, and using Eq. (8) to simplify, yields

$$\Delta \simeq \omega_4^2 (\mathcal{M} - \omega_2^2 \mathcal{I})^{-1} \left(\frac{U^{(4)} \vdots \hat{\pi}_4 \hat{\pi}_4 \hat{\pi}_4}{\chi_4} - \hat{\pi}_4 \right), \tag{D6}$$

which, once $(\mathcal{M} - \omega_2^2 \mathcal{I})^{-1}$ is written in diagonalized form, is equal to Eq. (17).

APPENDIX E: SUPPORTING DATA

In this Appendix, we have collected data that support various claims made in the main text.

---

[11] The same argument holds for cubic modes, the cost function of which features the third-order coefficient τ, which contains terms that scale as $|z_{ij}|^3$.
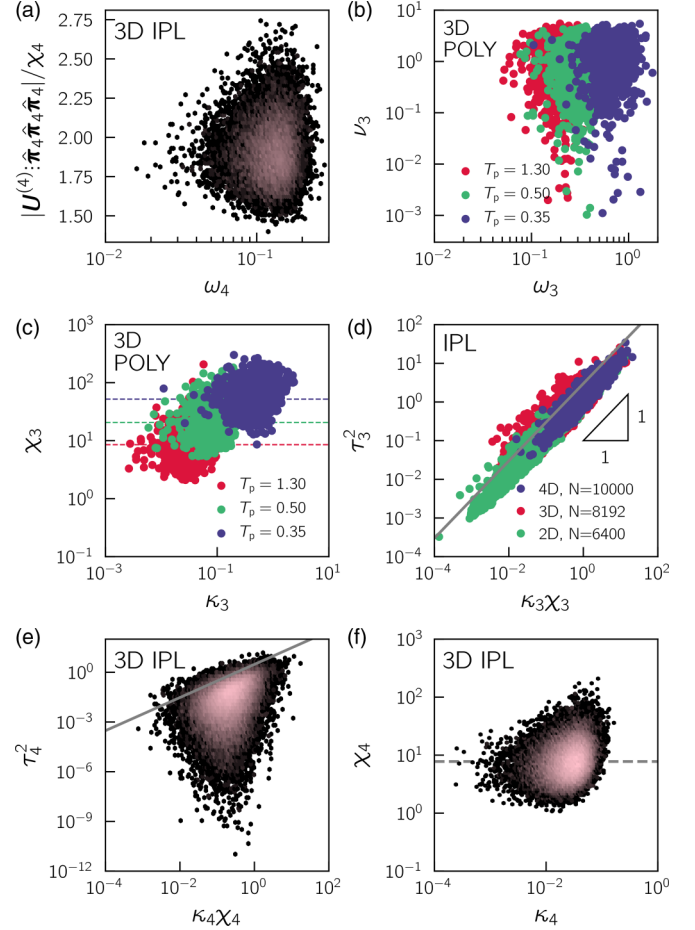

FIG. 9. (a) The magnitude of the field $U^{(4)} \vdots \hat{\pi}_4 \hat{\pi}_4 \hat{\pi}_4 / \chi_4$ is of order $O(1)$, independent of ω_4. (b) The shear-strain-coupling parameter $\nu_3 \equiv \frac{\partial^2 U}{\partial \gamma \partial x} \cdot \hat{\pi}_3$ associated with cubic modes $\hat{\pi}_3$ is independent of ω_3. (c) The fourth-order coefficient of cubic modes χ_3 is independent of ω_3. (d) The entire ensemble of cubic modes follows the relation $\tau_3^2 \sim \kappa_3 \chi_3$ in 2D, 3D, and 4D. (e) The ensemble of quartic modes does *not* follow this relation. (f) The fourth-order coefficient of quartic modes χ_4 is independent of ω_4. In panels (a), (e), and (f), the data are presented as a 2D histogram, where each bin is colored according to the number of hits in that bin (the color coding is the same as in Fig. 7).

[1] U. Buchenau, Y. M. Galperin, V. L. Gurevich, and H. R. Schober, Anharmonic potentials and vibrational localization in glasses, Phys. Rev. B **43**, 5039 (1991).

[2] U. Buchenau, Y. M. Galperin, V. L. Gurevich, D. A. Parshin, M. A. Ramos, and H. R. Schober, Interaction of soft modes and sound waves in glasses, Phys. Rev. B **46**, 2798 (1992).

[3] V. L. Gurevich, D. A. Parshin, and H. R. Schober, Anharmonicity, vibrational instability, and the boson peak in glasses, Phys. Rev. B **67**, 094203 (2003).

[4] B. B. Laird and H. R. Schober, Localized Low-Frequency Vibrational Modes in a Simple Model Glass, Phys. Rev. Lett. **66**, 636 (1991).

[5] H. Schober, C. Oligschleger, and B. Laird, Low-frequency vibrations and relaxations in glasses, J. Non-Cryst. Solids **156–158**, 965 (1993).

[6] H. R. Schober and C. Oligschleger, Low-frequency vibrations in a model glass, Phys. Rev. B **53**, 11469 (1996).

[7] C. S. O'Hern, L. E. Silbert, A. J. Liu, and S. R. Nagel, Jamming at zero temperature and zero applied stress: The epitome of disorder, Phys. Rev. E **68**, 011306 (2003).

[8] H. R. Schober and G. Ruocco, Size effects and quasilocalized vibrations, Philos. Mag. **84**, 1361 (2004).

[9] F. Leonforte, R. Boissière, A. Tanguy, J. P. Wittmer, and J.-L. Barrat, Continuum limit of amorphous elastic bodies. III. Three-dimensional systems, Phys. Rev. B **72**, 224206 (2005).

[10] N. Xu, V. Vitelli, A. J. Liu, and S. R. Nagel, Anharmonic and quasi-localized vibrations in jammed solids: Modes for mechanical failure, Europhys. Lett. **90**, 56001 (2010).

[11] M. Wyart, Scaling of phononic transport with connectivity in amorphous solids, Europhys. Lett. **89**, 64001 (2010).

[12] E. DeGiuli, A. Laversanne-Finot, G. During, E. Lerner, and M. Wyart, Effects of coordination and pressure on sound attenuation, boson peak and elasticity in amorphous solids, Soft Matter **10**, 5628 (2014).

[13] E. Lerner, G. Düring, and E. Bouchbinder, Statistics and Properties of Low-Frequency Vibrational Modes in Structural Glasses, Phys. Rev. Lett. **117**, 035501 (2016).

[14] L. Gartner and E. Lerner, Nonlinear modes disentangle glassy and Goldstone modes in structural glasses, SciPost Phys. **1**, 016 (2016).

[15] E. Lerner and E. Bouchbinder, Effect of instantaneous and continuous quenches on the density of vibrational modes in model glasses, Phys. Rev. E **96**, 020104(R) (2017).

[16] G. Kapteijns, E. Bouchbinder, and E. Lerner, Universal Non-phononic Density of States in 2D, 3D, and 4D Glasses, Phys. Rev. Lett. **121**, 055501 (2018).

[17] L. Wang, A. Ninarello, P. Guan, L. Berthier, G. Szamel, and E. Flenner, Low-frequency vibrational modes of stable glasses, Nat. Commun. **10**, 26 (2019).

[18] H. Mizuno, H. Shiba, and A. Ikeda, Continuum limit of the vibrational properties of amorphous solids, Proc. Natl. Acad. Sci. USA **114**, E9767 (2017).

[19] C. Rainone, E. Bouchbinder, and E. Lerner, Pinching a glass reveals key properties of its soft spots, arXiv:1911.07744.

[20] P. W. Anderson, B. I. Halperin, and C. M. Varma, Anomalous low-temperature thermal properties of glasses and spin glasses, Philos. Mag. **25**, 1 (1972).

[21] W. Phillips, Tunneling states in amorphous solids, J. Low Temp. Phys. **7**, 351 (1972).

[22] R. C. Zeller and R. O. Pohl, Thermal conductivity and specific heat of noncrystalline solids, Phys. Rev. B **4**, 2029 (1971).

[23] C. Maloney and A. Lemaître, Universal Breakdown of Elasticity at the Onset of Material Failure, Phys. Rev. Lett. **93**, 195501 (2004).

[24] E. Lerner, Micromechanics of nonlinear plastic modes, Phys. Rev. E **93**, 053004 (2016).

[25] H. Mizuno and A. Ikeda, Phonon transport and vibrational excitations in amorphous solids, Phys. Rev. E **98**, 062612 (2018).

[26] A. Moriel, G. Kapteijns, C. Rainone, J. Zylberg, E. Lerner, and E. Bouchbinder, Wave attenuation in glasses: Rayleigh and generalized-Rayleigh scattering scaling, J. Chem. Phys. **151**, 104503 (2019).

[27] A. Tanguy, B. Mantisi, and M. Tsamados, Vibrational modes as a predictor for plasticity in a model glass, Europhys. Lett. **90**, 16004 (2010).

[28] M. L. Manning and A. J. Liu, Vibrational Modes Identify Soft Spots in a Sheared Disordered Packing, Phys. Rev. Lett. **107**, 108302 (2011).

[29] J. Rottler, S. S. Schoenholz, and A. J. Liu, Predicting plasticity with soft vibrational modes: From dislocations to glasses, Phys. Rev. E **89**, 042304 (2014).

[30] L. Gartner and E. Lerner, Nonlinear plastic modes in disordered solids, Phys. Rev. E **93**, 011001(R) (2016).

[31] Z. Schwartzman-Nowik, E. Lerner, and E. Bouchbinder, Anisotropic structural predictor in glassy materials, Phys. Rev. E **99**, 060601(R) (2019).

[32] C. Oligschleger and H. R. Schober, Collective jumps in a soft-sphere glass, Phys. Rev. B **59**, 811 (1999).

[33] A. Widmer-Cooper, H. Perry, P. Harrowell, and D. R. Reichman, Irreversible reorganization in a supercooled liquid originates from localized soft modes, Nat. Phys. **4**, 711 (2008).

[34] A. Widmer-Cooper, H. Perry, P. Harrowell, and D. R. Reichman, Localized soft modes and the supercooled liquid's irreversible passage through its configuration space, J. Chem. Phys. **131**, 194508 (2009).

[35] J. Sethna, *Statistical Mechanics: Entropy, Order Parameters, and Complexity* (Oxford University, New York, 2006), Vol. 14.

[36] E. Bouchbinder and E. Lerner, Universal disorder-induced broadening of phonon bands: from disordered lattices to glasses, New J. Phys. **20**, 073022 (2018).

[37] C. Kittel, *Introduction to Solid State Physics* (Wiley, New York, 2005).

[38] E. Lerner, Finite-size effects in the nonphononic density of states in computer glasses, Phys. Rev. E **101**, 032120 (2020).

[39] J. Zylberg, E. Lerner, Y. Bar-Sinai, and E. Bouchbinder, Local thermal energy as a structural indicator in glasses, Proc. Natl. Acad. Sci. USA **114**, 7289 (2017).

[40] E. Lerner, Mechanical properties of simple computer glasses, J. Non-Cryst. Solids **522**, 119570 (2019).

[41] A. Ninarello, L. Berthier, and D. Coslovich, Models and Algorithms for the Next Generation of Glass Transition Studies, Phys. Rev. X **7**, 021039 (2017).

[42] N.-H. Tsai, F. F. Abraham, and G. Pound, The structure and thermodynamics of binary microclusters: A Monte Carlo simulation, Surf. Sci. **77**, 465 (1978).

[43] D. Gazzillo and G. Pastore, Equation of state for symmetric non-additive hard-sphere fluids: An approximate analytic expression and new Monte Carlo results, Chem. Phys. Lett. **159**, 388 (1989).

[44] T. S. Grigera and G. Parisi, Fast Monte Carlo algorithm for supercooled soft spheres, Phys. Rev. E **63**, 045102(R) (2001).

[45] M. L. Falk and J. S. Langer, Dynamics of viscoplastic deformation in amorphous solids, Phys. Rev. E **57**, 7192 (1998).

[46] M. Shimada, H. Mizuno, L. Berthier, and A. Ikeda, Low-frequency vibrations of jammed packings in large spatial dimensions, arXiv:1910.07238.

[47] G. Kapteijns, W. Ji, C. Brito, M. Wyart, and E. Lerner, Fast generation of ultrastable computer glasses by minimization of an augmented potential energy, Phys. Rev. E **99**, 012106 (2019).

[48] H. Jónsson, G. Mills, and K. W. Jacobsen, Nudged elastic band method for finding minimum energy paths of transitions, *Classical and Quantum Dynamics in Condensed Phase Simulations* (World Scientific, Singapore, 1997), Chap. 16.

[49] G. Henkelman, B. P. Uberuaga, and H. Jónsson, A climbing image nudged elastic band method for finding saddle points and minimum energy paths, J. Chem. Phys. **113**, 9901 (2000).

[50] N. Mousseau and G. T. Barkema, Traveling through potential energy landscapes of disordered materials: The activation-relaxation technique, Phys. Rev. E **57**, 2419 (1998).

[51] E. Cances, F. Legoll, M.-C. Marinica, K. Minoukadeh, and F. Willaime, Some improvements of the activation-relaxation technique method for finding transition pathways on potential energy surfaces, J. Chem. Phys. **130**, 114711 (2009).

[52] N. Mousseau, L. K. Béland, P. Brommer, J.-F. Joly, F. El-Mellouhi, E. Machado-Charry, M.-C. Marinica, and P. Pochet, The activation-relaxation technique: Art nouveau and kinetic art, J. At. Mol. Opt. Phys. **2012**, 925278 (2012).

[53] C. Maloney and A. Lemaître, Subextensive Scaling in the Athermal, Quasistatic Limit of Amorphous Matter in Plastic Shear Flow, Phys. Rev. Lett. **93**, 016001 (2004).

[54] C. E. Maloney and A. Lemaître, Amorphous systems in athermal, quasistatic shear, Phys. Rev. E **74**, 016118 (2006).

[55] S. Karmakar, E. Lerner, and I. Procaccia, Statistical physics of the yielding transition in amorphous solids, Phys. Rev. E **82**, 055103(R) (2010).

[56] K. M. Salerno, C. E. Maloney, and M. O. Robbins, Avalanches in Strained Amorphous Solids: Does Inertia Destroy Critical Behavior? Phys. Rev. Lett. **109**, 105703 (2012).

[57] J. Lin, A. Saade, E. Lerner, A. Rosso, and M. Wyart, On the density of shear transformations in amorphous solids, Europhys. Lett. **105**, 26003 (2014).

[58] H. G. E. Hentschel, P. K. Jaiswal, I. Procaccia, and S. Sastry, Stochastic approach to plasticity and yield in amorphous solids, Phys. Rev. E **92**, 062302 (2015).

[59] J. Lin and M. Wyart, Mean-Field Description of Plastic Flow in Amorphous Solids, Phys. Rev. X **6**, 011005 (2016).

[60] P. Leishangthem, A. D. S. Parmar, and S. Sastry, The yielding transition in amorphous solids under oscillatory shear deformation, Nat. Commun. **8**, 14653 (2017).

[61] E. Lerner, I. Procaccia, C. Rainone, and M. Singh, Protocol dependence of plasticity in ultrastable amorphous solids, Phys. Rev. E **98**, 063001 (2018).

[62] B. Shang, P. Guan, and J.-L. Barrat, Elastic avalanches reveal marginal behaviour in amorphous solids, arXiv:1908.08820.

[63] W. Ji, M. Popović, T. W. J. de Geus, E. Lerner, and M. Wyart, Theory for the density of interacting quasilocalized modes in amorphous solids, Phys. Rev. E **99**, 023003 (2019).

[64] A. J. Liu and S. R. Nagel, The jamming transition and the marginally jammed solid, Annu. Rev. Condens. Matter Phys. **1**, 347 (2010).

[65] M. van Hecke, Jamming of soft particles: Geometry, mechanics, scaling and isostaticity, J. Phys.: Condens. Matter **22**, 033101 (2010).

[66] A. J. Liu, S. R. Nagel, W. Van Saarloos, and M. Wyart, The jamming scenario-an introduction and outlook, *Dynamical Heterogeneities in Glasses, Colloids, and Granular Media* (Oxford University, New York, 2011).

[67] P. Charbonneau, J. Kurchan, G. Parisi, P. Urbani, and F. Zamponi, Fractal free energy landscapes in structural glasses, Nat. Commun. **5**, 3725 (2014).

[68] C. Scalliet, L. Berthier, and F. Zamponi, Nature of excitations and defects in structural glasses, Nat. Commun. **10**, 5102 (2019).

[69] M. Shimada, H. Mizuno, M. Wyart, and A. Ikeda, Spatial structure of quasilocalized vibrations in nearly jammed amorphous solids, Phys. Rev. E **98**, 060901(R) (2018).

[70] E. Lerner and E. Bouchbinder, A characteristic energy scale in glasses, J. Chem. Phys. **148**, 214502 (2018).

[71] L. Yan, E. DeGiuli, and M. Wyart, On variational arguments for vibrational modes near jamming, Europhys. Lett. **114**, 26003 (2016).

[72] R. B. Lehoucq, D. C. Sorensen, and C. Yang, *ARPACK Users' Guide: Solution of Large-Scale Eigenvalue Problems with Implicitly Restarted Arnoldi Methods* (SIAM, New York, 1998), Vol. 6.

[73] S. Karmakar, E. Lerner, and I. Procaccia, Athermal nonlinear elastic constants of amorphous solids, Phys. Rev. E **82**, 026105 (2010).

[74] D. MacKay, MACOPT optimizer, http://www.inference.org.uk/mackay/c/macopt.html, 2004 (2019-12-12).